NAR Cancer, 2025, **7**, zcaf006
https://doi.org/10.1093/narcan/zcaf006
Cancer Gene Regulation, Chromatin, and Epigenetics

OXFORD

The IGF2BP1 oncogene is a druggable m^{6}A-dependent enhancer of YAP1-driven gene expression in ovarian cancer

Annekatrin Schott[1], Theresa Simon[1], Simon Müller[2], Alexander Rausch[1], Bianca Busch[1], Markus Glaß[1], Danny Misiak[1], Mohammad Dipto[1], Hend Elrewany[1], Lara Meret Peters[1], Sunita Tripathee[1], Ehab Ghazy[3], Florian Müller[1], Robin Benedikt Rolnik[1], Marcell Lederer[1], Ali Hmedat[1,4], Martina Vetter[5], Markus Wallwiener[5], Wolfgang Sippl[3], Stefan Hüttelmaier[1,†], Nadine Bley[1,*,†]

[1]Institute of Molecular Medicine, Section for Molecular Cell Biology, Faculty of Medicine, Martin Luther University Halle-Wittenberg, 06120 Halle, Germany
[2]New York Genome Center, 10013 New York, NY, United States; Department of Biology, New York University, 10003 New York, NY, United States
[3]Department of Pharmaceutical Chemistry and Bioanalytics, Institute of Pharmacy, Martin Luther University Halle-Wittenberg, Kurt-Mothes-Straße 3, 01620 Halle (Saale), Germany
[4]Department of Pharmaceutics and Pharmaceutical Technology, Faculty of Pharmacy, Yarmouk University, 21163 Irbid, Jordan
[5]Department of Gynecology, University Hospital, Martin Luther University Halle-Wittenberg, Ernst-Grube-Straße 40, 01620 Halle (Saale), Germany

*To whom correspondence should be addressed. Email: nadine.stoehr@medizin.uni-halle.de
†These authors shared correspondence.

Abstract

The Hippo/YAP1 signaling pathway regulates normal development by controlling contact inhibition of growth. In cancer, YAP1 activation is often dysregulated, leading to excessive tumor growth and metastasis. SRC kinase can cross talk to Hippo signaling by disrupting adherens junctions, repressing the Hippo cascade, or activating YAP1 to promote proliferation. Here, we demonstrate that the IGF2 messenger RNA-binding protein 1 (IGF2BP1) impedes the repression of YAP1 by Hippo signaling in carcinomas. IGF2BP1 stabilizes the YAP1 messenger RNA (mRNA) and enhances YAP1 protein synthesis through an m^{6}A-dependent interaction with the 3′ untranslated region of the YAP1 mRNA, thereby increasing YAP1/TAZ-driven transcription to bypass contact inhibition of tumor cell growth. Inhibiting IGF2BP1–mRNA binding using BTYNB reduces YAP1 levels and transcriptional activity, leading to significant growth inhibition in carcinoma cells and ovarian cancer organoids. In contrast, SRC inhibition with Saracatinib fails to inhibit YAP1/TAZ-driven transcription and cell growth in general. This is particularly significant in de-differentiated, rather mesenchymal carcinoma-derived cells, which exhibit high IGF2BP1 and YAP1 expression, rendering them less reliant on SRC-directed growth stimulation. In such invasive carcinoma models, the combined inhibition of SRC, IGF2BP1, and YAP1/TAZ proved superior over monotherapies. These findings highlight the therapeutic potential of targeting IGF2BP1, a key regulator of oncogenic transcription networks.

Graphical abstract

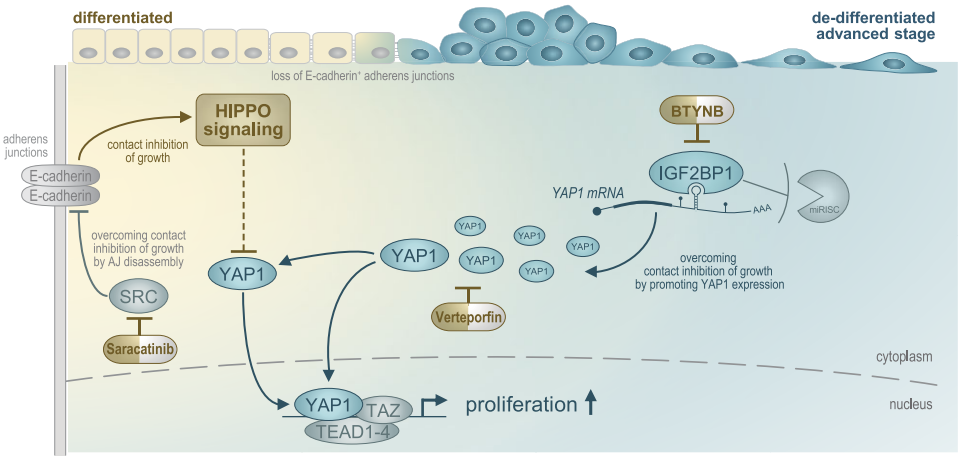

Received: October 16, 2024. **Revised:** February 2, 2025. **Editorial Decision:** February 7, 2025. **Accepted:** February 13, 2025

Introduction

Epithelial ovarian carcinoma (EOC) remains the second most common but most devastating gynecological malignancy in women, with 5-year survival rates of ∼30% for women diagnosed with an invasive disease [1, 2]. The ovary is a highly dynamic tissue that undergoes extensive remodeling during each reproductive cycle, a process primarily regulated by endocrine signaling and various intracellular signaling pathways that control follicle development growth, and fate [3]. One key pathway in normal follicle development—and frequently deregulated in gynecological malignancies, particularly EOC—is the Hippo signaling pathway [3, 4]. This intracellular signaling cascade involves a series of protein kinases, which limit the activity of the transcriptional regulators YAP1 and TAZ (WWTR1). These regulators promote the expression of proliferation-related genes in conjunction with TEAD transcription factors [3]. Accordingly, Hippo signaling plays a critical role in controlling organ size and maintaining tissue homeostasis. Although lacking dedicated upstream receptors, the Hippo pathway integrates a variety of guidance cues resulting in the protein kinase dependent restriction of YAP1/TAZ-driven gene synthesis. This inhibitory signaling relies on retaining YAP1/TAZ in the cytoplasm, due to partial association with cytoskeletal proteins like CTNNA1 (α-catenin) in E-cadherin-positive adherens junctions (AJs) [5] and multifunctional 14-3-3 proteins [6, 7], as well as promoting YAP1/TAZ protein decay. The deregulation of YAP1/TAZ activity in cancer is linked to aggressive tumor growth due to the loss of contact inhibition [5], the promotion of cancer stem-cell-like properties, enhanced immune evasion, stimulated angiogenesis, and ultimately metastasis [8, 9]. Consequently, considerable efforts aim at developing therapeutic strategies to impair YAP1/TAZ signaling in cancer. These include approaches to impair the transcriptional activity of YAP1/TAZ by elevating cytoplasmic retention and protein decay via 14-3-3 proteins and/or p62, the proposed mechanisms of Verteporfin [10, 11]. More recently, therapeutic efforts have focused on disrupting the interaction between YAP1/TAZ and TEADs, serving as transcriptional co-factors in activating gene synthesis. The discovery of TEAD autopalmitoylation has further stimulated interest in targeting this post-translational modification, as it regulates TEAD activity, subcellular localization, and stability [12].

Consistent with the upregulation of YAP1 in various, if not most, malignancies, post-transcriptional downregulation of YAP1 by tumor-suppressive microRNAs (miRNAs) has been reported. One key conserved mechanism antagonizing excessive YAP1 abundance in cancer cells involves miRs-15/16-5p, which impair tumor growth and invasion by downregulating YAP1 [13]. In glioma, recent studies have proposed that the opposite, an enhancement of YAP1 abundance, is stimulated by the oncofetal IGF2 messenger RNA-binding protein 1 (IGF2BP1) [14]. The IGF2BP1 is a conserved oncogene upregulated in advanced, high-risk diseases [15, 16], where it promotes the expression of various tumorigenic factors such as MYC and MYCN [17–19], by preventing the decay of their respective messenger RNAs (mRNAs) [20, 21]. A primary function of IGF2BPs in cancer is to impede mRNA silencing by miRNAs, either through sequestering target transcripts in dormant IGF2BP-associated mRNPs or by directly shielding miRNA-targeting sites [22–25]. Recent studies have shown that this mRNA-stabilizing role of IGF2BP1 is enhanced by METTL3-directed m^6A modifications, which increase IGF2BP1's association with various target mRNAs, such as MYC and E2F1-3, thereby promoting the expression of these oncogenic drivers [18, 25–27]. In EOC and other malignancies, IGF2BP1 has been shown to foster proliferation, epithelial–mesenchymal transition (EMT), invasive potential, and metastasis by enhancing stem-cell-like properties [19, 24, 28–30]. Importantly, the discovery of BTYNB, a small molecule that disrupts IGF2BP1–RNA interactions [31], has demonstrated that IGF2BP1 is a druggable oncogene. The therapeutic potential of targeting IGF2BP1 in cancer has since been validated in various carcinoma and neuroblastoma models [17, 26, 32, 33], spurring the development of additional small-molecule inhibitors [34–36].

Although most of IGF2BP1's oncogenic roles involve the stabilization of target mRNAs, recent studies in EOC models have uncovered an unexpected function of IGF2BP1, the ligand-binding-induced activation of SRC kinase. This activation occurs in an RNA-independent manner, as IGF2BP1 binding to the SH3 domain of SRC promotes autoactivation of the kinase. SRC activation by IGF2BP1 promotes AJ disassembly, EMT, and tumor cell invasion [37]. Notably, SRC family kinases can interfere with Hippo signaling through multiple mechanisms: (i) by promoting the disassembly of AJs to overcome contact inhibition of growth; (ii) by limiting LATS1 activity to activate YAP1; and (iii) by phosphorylating YES1 to promote its transcriptional activity [38]. SRC inhibition (SRCi) by Saracatinib effectively countered IGF2BP1-driven invasion but was less effective in suppressing spheroid growth [37]. Moreover, phase II studies across various cancer types, including platinum-resistant EOC (NCT01196741), demonstrated limited therapeutic efficacy of Saracatinib as a monotherapy [39–41]. The resistance to Saracatinib was linked to the activation of pro-proliferative pathways [42].

Building on the evidence of IGF2BP1-stimulated YAP1 expression in glioma [14] and SRC-driven increases in YAP1 activity [43], we hypothesized that IGF2BP1 serves as a druggable enhancer of YAP1/TAZ-driven progression in EOC and impacts the efficacy of SRC-targeted therapies. Supporting this hypothesis, we demonstrate that IGF2BP1 enhances YAP1 levels in EOC and other carcinomas through a highly conserved mechanism. This enhancement relies on the 3′ untranslated region (3′UTR)-mediated stabilization of YAP1 mRNA by IGF2BP1, which is fostered by METTL3-driven m^6A modifications. Consistently, disrupting IGF2BP1–RNA interactions with BTYNB suppresses IGF2BP1-induced YAP1 expression and inhibits the invasive growth of EOC tumor cells and organoids. In contrast, SRCi with Saracatinib only showed limited and less conserved efficacy on YAP1-driven tumor growth in carcinoma models, but effectively impairing invasion. Combining SRCi with broadly growth-inhibitory compounds such as Verteporfin or BTYNB significantly enhances efficacy in YAP1-driven cancer cells and EOC-derived organoids, enabling an up to 10-fold reduction in effective dosage of each compound.

Materials and methods

Cell culture, transfection, and transduction

ES-2 (RRID: CVCL_3509), A549 (RRID: CVCL_0023), SAS (RRID: CVCL_1675), HUH-7 (RRID: CVCL_0336), PANC-1 (RRID: CVCL_0480), HEK293T/17 (ATCC,

RRID: CVCL_1926), HEK293T/R-Spondin-1 (RRID: CVCL_RU09), and L-Wnt-3A (RRID: CVCL_0635) cells were cultured in Dulbecco's modified Eagle's medium (DMEM) supplemented with 10% fetal bovine serum and 1% GlutaMax at 37°C in 5% CO_2. For HEK293T/R-Spondin-1, culture medium was additionally supplemented with 300 µg/ml Zeocin (Thermo Fisher), L-Wnt-3A were cultured under G418 selection (400 µg/ml; Thermo Fisher). To produce R-Spondin-1 or Wnt-3A pre-conditioned medium, cells were grown in Advanced DMEM/F-12 supplemented with 1% HEPES, 1% GlutaMax, and 1% Penicillin/Streptomycin for 48 h (all Thermo Fisher).

Transfection of cells with DNA or short interfering RNAs (siRNAs) was carried out using Lipofectamine 3000 or Lipofectamine RNAiMAX (Thermo Fisher Scientific) according to the manufacturer's instructions. For luciferase reporter assays, 1×10^5 cells were transfected with Lipofectamine 3000 and either pmirGLO or NanoLuc® plasmids. For genomic deletions via CRISPR/Cas9, 5×10^5 cells were transfected with Lipofectamine 3000, Cas9-, and single guide RNA (sgRNA)-encoding plasmids (see "CRISPR/Cas9" section). For gene-specific depletion using siRNAs, 8×10^5 cells were transfected with 9 µl Lipofectamine RNAiMAX and 15 nM siRNAs.

For the production of lentiviral particles, 3.5×10^6 HEK293T/17 cells were transfected with Lipofectamine 3000 along with the packaging plasmids psPax2 (Addgene: Plasmid #12260), pMD2.G (Addgene: Plasmid #12259), and the lentiviral expression pLVX (GFP, IGF2BP1, or IGF2BP1-KHmut), or pHAGE (EV or YAP1) using 15 µl Lipofectamine 3000. Lentiviral particle-containing supernatants were collected 24 and 48 h post-transfection of HEK293T/17 cells. Titers were assessed 48 h post-infection of HEK293T/17 cells by flow cytometry using a MACSQuantX Analyzer (Miltenyi Biotec). Lentiviral transduction for downstream experiments was performed at a multiplicity of infection of 10. Plasmids and siRNAs used are summarized in Supplementary Table S1.

The inhibitors BTYNB (Cayman Chemical, #CAY25623), Saracatinib (Selleckchem, #S1006), and Verteporfin (Selleckchem, #S1786) were used at the indicated concentrations. For RNA decay analyses, cells were treated with 5 µM Actinomycin D (Sigma–Aldrich) for the indicated timepoints.

Organoid culture

In this study, we included an organoid derived from a patient sample diagnosed with undifferentiated high-grade serous ovarian carcinoma (stage IVa) at the age of 57. Ethical approval was obtained from the Ethics Committee of the Medical Faculty of Martin Luther University Halle-Wittenberg (208/17.06.09/12), and written informed consent was provided by the patient. The tumor tissue was minced and dissociated using the human tumor dissociation kit (Miltenyi Biotec) and subsequently filtered through a 100-µm cell strainer. Cells were embedded in 50–100 µl Matrigel® (Corning) domes and cultured with weekly passaging in organoid medium (Advanced DMEM/F-15 supplemented with 10% R-Spondin1- and 10% Wnt-3A-pre-conditioned medium, 1% HEPES, 1% GlutaMax, 1% Penicillin/Streptomycin, 1× B27 supplement, 1× N-2 supplement, 10 mM Nicotinamide, 1.25 mM N-acetyl-cysteine, 10 µM Forskolin, 10 ng/ml FGF-10, 10 ng/ml Noggin, 5 ng/ml EGF, 5 µM Y27632, 500 nM SB431542, 200 nM Hydrocortisone, 100 nM Estradiol, 0.2% Primocin). Assays were conducted between passages 5 and 10. For experimental assays, cells were harvested in ice-cold organoid medium, centrifuged at 300 × *g* for 5 min at 4°C, and seeded in 5 µl Matrigel® domes per 96-well plate. Organoids were cultured for 48 h before treatment with the indicated compounds at respective concentrations. Organoid growth was monitored over 72 h using an Incucyte S3 system (Sartorius) equipped with the organoid analysis module. Growth rates were determined by normalizing the segmented organoid area to the starting point of compound treatment. For all treatments, biological triplicates were analyzed.

Cell proliferation, spheroid invasion, and compound treatments

Analyses of 2D cell proliferation and 3D spheroid invasion assays were performed as recently described [37]. For 2D proliferation, cells were seeded at indicated densities and cell viability was determined by Cell-Titer-Glo® assay (Promega) for indicated timepoints. Average growth rate per day was determined according to the following formula: $GR = \ln(X_t/X_0)/\Delta t$ with GR accounting for the average growth rate, X for the cell number, and t for the growth time in days. Doubling times (in hours) were calculated by $DT = 24/GR$, where DT denotes doubling time. For compound treatments, 2×10^3 cells were seeded per well in 96-well plates (TPP) 24 h before treatment with compounds at the indicated concentrations for 72 h. Cell proliferation was analyzed 3-days post-seeding using bright-field microscopy with an Incucyte® S3 (Sartorius). Cell growth and viability were assessed using the AI Cell Health software module (Sartorius) and validated with the Cell-Titer-Glo® assay (Promega). EC_{50} values were determined using GraphPad Prism with four-parameter dose-response fitting. For the analysis of synergy among BTYNB, Saracatinib, and Verteporfin, the viability of ES-2 cells was determined 72 h upon drug exposure using Cell-Titer-Glo® drug matrix screen at indicated concentrations. Synergy relief maps were generated using the SynergyFinder web application (https://synergyfinder.fimm.fi, [44]) and the highest single-agent (HSA) [45] method. Additivity is defined for delta scores between 0 and 10, whereas synergy is defined for delta scores between 10 and 100.

For 3D spheroid invasion assays, 2×10^3 cells in 50-µl culture medium per well were seeded in Corning® 96-Well Clear Round Bottom Ultra Low Attachment microplates and centrifuged for 3 min at 300 × *g* to promote spheroid formation. Twenty-four hours post-seeding, spheroids were embedded in 50 µl Matrigel® (Corning) and centrifuged again for 3 min at 300 × *g* and 4°C. After Matrigel solidification (1 h at 37°C), compounds were added in 100-µl culture medium at the indicated final concentrations. Invasion was monitored for 72 h using the spheroid module of the Incucyte® S3 (Sartorius), and the invasive area was quantified by segmentation, shown relative to DMSO control when applicable. All experiments were performed in biological triplicates.

Plasmids, siRNAs, and CRISPR/Cas9

Plasmid generation including vectors, respective templates, and restrictions sites is summarized in Supplementary Table S1. All constructs were validated by sequencing. For CRISPR/Cas9-mediated deletion of the YAP1-3′UTR, 5×10^5 ES-2 cells were transfected with two sgRNA-encoding plasmids (psg_RFP_YAP1_3P1 and psg_RFP_YAP1_3P2) and a Cas9 nuclease encoding plasmid (pcDNA-Cas9-T2A-GFP).

RFP-/GFP-positive cells were isolated by single-cell sorting using a FACS Melody cell sorter (BD Bioscience) 48 h post-transfection. Knockout in populations derived from single-cell clones was confirmed by polymerase chain reaction (PCR) and Sanger sequencing. IGF2BP1 and METTL3 knockout ES-2 clones have been described previously [24, 26].

Luciferase assay

Luciferase activity was analyzed 72 h post-transfection of luciferase-encoding reporters using the Dual-Glo® assay (Promega), essentially as previously described [26]. For YAP1-3′UTR reporters, firefly luciferase (FFL) activities were normalized to renilla luciferase activities to obtain relative luminescence units (RLU). RLU ratios were further normalized to control populations and the luciferase empty vector control. For YAP1/TAZ-binding element reporters, NanoLuc® luciferase activities were normalized to FFL activities, with RLU calculated relative to control conditions and a control reporter containing only a minimal promoter.

IGF2BP1 CLIP analyses, m^{6}A modifications, and RNA co-immunoprecipitation

The analyses of IGF2BP1 cumulated CLIP scores were previously described by Müller *et al.* [24]. m^{6}A modifications of the YAP1-3′UTR based on m^{6}A-seq and MeRIP-seq methods were derived from RMBase v2.0 (https://bioinformaticsscience.cn/rmbase/) [46, 47]. For RNA co-immunoprecipitation (RIP), cell extracts (1×10^7 cells per condition) were prepared on ice using RIP buffer [10 mM HEPES, 150 mM KCl, 5 mM $MgCl_2$, 0.5% NP40 (pH 7.0)]. Cleared lysates were incubated with anti-GFP antibodies (Roche) and Protein G Dynabeads (Life Technologies) for 30 min at room temperature (RT). After three washing steps with RIP buffer, protein–RNA complexes were eluted by addition of 1% sodium dodecyl sulfate at 65°C for 10 min. Protein enrichment was analyzed by western blotting, and co-purified RNAs were extracted using TRIzol® and analyzed by RT-qPCR (reverse transcription and quantitative polymerase chain reaction).

RNA isolation, RT-qPCR, and m^{6}A RNA capture

Total RNA from cell line experiments was extracted using TRIzol®. Complementary DNA synthesis was performed with M-MLV Reverse Transcriptase (Promega), using either random hexamer primers or oligo (dT) primers for RNA turnover experiments. qPCR analysis was conducted as previously described [26]. Primer sequences are provided in Supplementary Table S1. Relative RNA abundance was calculated using the ΔΔCt method, as described previously [48]. Changes in global m^{6}A modifications following METTL3 knockout compared with parental ES-2 cells were determined using the colorimetric m^{6}A RNA methylation quantification kit (Abcam) according to the manufacturer's instructions using fresh TRIzol®-isolated RNA.

RNA sequencing and data processing

RNA integrity was assessed using a Bioanalyzer 2100 (Agilent). RNA sequencing (RNA-seq) libraries were prepared according to the manufacturer's instructions. For mRNA-seq, total RNA was used as input for poly (A) enrichment with oligo (dT) beads. Library preparation and sequencing were performed by Novogene (Hong Kong) on the Illumina HiSeq or NovaSeq platforms. Low-quality read ends and residual sequencing adapter fragments were trimmed using Cutadapt. Reads were aligned to the human genome (UCSC GRCh37 or 38) using TopHat2 or HISAT2, respectively. Gene-mapped reads were summarized using FeatureCounts based on Ensembl (GRCh37.75 or GRCH38.89). Differential gene expression (DE) analysis was conducted with edgeR using trimmed mean of M-values (TMM) normalization, as previously described [26]. Further details are available associated to the respective datasets GSE109605, GSE116136, and GSE283587.

Public sequencing data, correlations, over-representation, and gene set enrichment analyses

Gene expression profiles from healthy ovarian samples were obtained as read counts from the GTEx portal (https://gtexportal.org/; GTEx v7). Gene expression profiles from TCGA ovarian cancer samples were obtained as read counts from the GDC data portal (https://portal.gdc.cancer.gov/). DE was determined using the R package edgeR [49] utilizing TMM [50] normalization. EdgeR's exactTest function was applied for testing for differentially expressed genes. Gene expression data for EOC-derived cell lines from the CCLE dataset were obtained as RNA-Seq by Expectation-Maximization (RSEM)-normalized $\log_2$ transformed gene expression data from (https://r2.amc.nl). Over-representation analyses (ORAs) of KEGG pathways upon DE of IGF2BP1 correlated genes (TCGA-OV-304 dataset) were carried out using a significance cutoff of false discovery rate (FDR) < 0.05 using the R2 platform (https://r2.amc.nl). RSEM-normalized $\log_2$ transformed gene expression data for indicated TCGA-RNA-seq datasets were obtained from the R2 and Pearson correlation to IGF2BP1 was determined. Gene set enrichment analysis (GSEA) was performed on pre-ranked lists using the GSEA-software (v3.0 [51]) with MSigDB (v7.0 [52]) gene sets for Hallmarks and KEGG pathways. All protein-coding genes were ranked according to the Pearson correlation coefficient with IGF2BP1 in indicated TCGA-RNA-seq datasets or the fold change determined upon IGF2BP1 knockdown by RNA-seq. The YAP1 target gene set was assembled according to Galli *et al.* [53].

Kaplan–Meier analyses

Kaplan–Meier analyses were conducted to assess differences in progression-free survival based on IGF2BP1 expression in EOC, using the KMplot database (https://kmplot.com) [54]. The analysis applied a median cutoff and included all available datasets.

Western blot and biotin labeling of newly synthesized proteins

Protein expression was assessed by western blotting as previously described [37]. Primary and fluorophore-conjugated secondary antibodies are listed in Supplementary Table S1. Vinculin (VCL) was used as loading control to determine relative changes in protein levels. To analyze density-dependent differences in protein translation, labeling of newly synthesized proteins was required. Cells were seeded at two different densities (25 000 and 100 000 cells/cm^2) and cultured for 48 h. Following this, the growth medium was replaced with

methionine-free medium for 30 min, after which 50 μM of the methionine analog Click-iT® AHA (L-azidohomoalanine; Thermo Fisher) was added for 2 h. Cells were harvested and newly synthesized proteins incorporating AHA were subsequently labeled with biotin using the Click-iT® Biotin Protein Analysis Detection Kit (Thermo Fisher) and analyzed by western blotting using Atto 800-Streptavidin for detection and Ponceau staining to ensure equal loading.

Protein purification

Codon optimized IGF2BP1 was expressed in *Escherichia coli* strain BL21-CodonPlus (DE3)-RIPL (StrataGene) and purified as previously described [55] with slight modification. Briefly, bacteria were lysed in lysis buffer (50 mM phosphate buffer, 1% Triton, 700 mM NaCl, 5 mM ethylene glycol-bis(β-aminoethyl ether)-N,N,N′,N′-tetraacetic acid (EGTA), 5 mM ethylenediaminetetraacetic acid (EDTA), 1 mM Dithiothreitol (DTT)) supplemented with protease inhibitors and lysozyme. After sonification and centrifugation at 8000 × *g* for 20 min, the cell extracts were incubated with glutathione-sepharose for 2 h at 4°C. After extensive washing with lysis buffer, protein was incubated with PreScission protease (GE Healthcare) over night and eluted (50 mM phosphate buffer, 600 mM NaCl, 10 mM EDTA, 0.1% Triton, 1 mM DTT). Eluted proteins were further purified by linear salt elution from Heparin column using an Äkta-FPLC (GE Healthcare) [55]. Eluted proteins were desalted into storage buffer [50 mM HEPES buffer, 300 mM NaCl, 3 mM $MgCl_2$, 10% Glycerol (pH 7.4)] and stored at −80°C.

Spectral shift/micro-scale thermophoresis

Recombinant full-length IGF2BP1 protein was labeled with RED-Tris-NTA dye using a Monolith NT His-Tag Labelling Kit (NanoTemper). Labeled proteins were centrifuged at 15 000 × *g* for 10 min at 4°C to remove aggregates. Reactions (20 μl) containing 50 nM labeled IGF2BP1 protein were incubated with indicated RNA probe concentrations in reaction buffer (1× PBST (phosphat buffered saline/Tween-20), 1 mM DTT) at RT for 10 min before loading into standard capillaries (NanoTemper) for measurement in the Monolith X (MM-240) (NanoTemper) under standard reading conditions [100% LED power and medium micro-scale thermophoresis (MST) power]. Results were analyzed using the MO Control v2.6.6 software (NanoTemper) at the 2.5 s timepoint for curve fitting to determine the K_d. Raw data were extracted and analyzed via GraphPad Prism v10.

Immunostaining

To monitor cell growth in multiple layers, cells were cultured at a high seeding density (100 000 cells/cm^2) on coverslips. Cells were fixed with 4% paraformaldehyde (PFA) for 15 min at RT, permeabilized with 0.5% Triton X-100 in phosphate-buffered saline for 5 min, and stained with DAPI (Sigma–Aldrich) to label the nuclei as well as Phalloidin–Atto 647 (ThermoFisher) to stain the F-actin cytoskeleton. Image stacks were acquired using an SP8X confocal microscope (Leica) equipped with a 405-nm diode, a white light laser, and HyD detectors under standard settings. 3D projections were generated using LAS-X software and are presented in glow-over LUT (DAPI) and F-actin in cyan.

Analysis of IGF2BP1 and YAP1 protein expression in an EOC-tissue microarray

A tissue microarray (TMA) containing 35 primary tumors and corresponding metastases from the greater omentum (Supplementary Table S2; OV812; tissuearray.com), derived from HGSC samples, was stained using the Opal7 kit (Akoya) to analyze IGF2BP1 and YAP1 protein expression. The TMA was incubated at 65°C for 2 h, followed by dewaxing with xylene (3 × 10 min) and a graded ethanol series. Tissue fixation was carried out with 4% PFA for 20 min. Heat-induced epitope retrieval was performed in pH 9 Tris buffer (Akoya) at 95°C for 20 min. Cyclic antibody staining was then conducted manually using the Opal7 kit, with the following antibodies: IGF2BP1 (pH 9; 1:50 [37]), YAP1 (pH 9; 1:50; Santa Cruz), pan-Cytokeratin (pan-CK; pH 6; 1:300; BioLegend), and spectral DAPI.

Images were acquired using a Leica SP8X confocal microscope equipped with a white light laser. Sequential imaging settings with HyD detectors, narrow detection bandwidth, and time gating were employed. Image segmentation and analysis were performed using QuPath! (https://qupath.readthedocs.io/en/0.5/) [56].

Statistics

All experiments were performed at least in biological triplicates. Statistical significance was tested by a parametric Student's *t*-test on equally distributed data. Otherwise, a non-parametric Mann–Whitney-test was performed.

Results

IGF2BP1 enhances ovarian cancer growth by fostering YAP/TAZ-driven transcription

The oncofetal RNA-binding protein IGF2BP1 is frequently overexpressed in various solid cancers including EOC, promoting mesenchymal-like tumor cell properties [28], the invasive growth of carcinomas [24], and metastasis (Fig. 1A and B and Supplementary Fig. S1A). Its expression is correlated with the mesenchymal and proliferative C5 subtype of ovarian carcinoma and poor patient outcomes (Supplementary Fig. S1B and C) [37, 57]. Beyond post-transcriptional stimulation of mesenchymal factors, e.g. LEF1 and SLUG [28], IGF2BP1 enhances EMT through the disassembly of AJs via the protein–ligand binding-induced activation of SRC kinase [37]. These findings imply that IGF2BP1 also impairs contact inhibition of tumor growth.

To investigate this, overexpression and depletion studies were conducted using EOC-derived ES-2 (Supplementary Fig. S1D). The impact of stable IGF2BP1 overexpression (G-I1, GFP-IGF2BP1) or IGF2BP1 depletion (Fig. 1C) on contact inhibition was assessed by monitoring the 2D growth at varying initial cell densities (Fig. 1D and Supplementary Fig. S1E). IGF2BP1 depletion significantly reduced cell growth, particularly at high cell densities. Conversely, enforced IGF2BP1 expression conferred a notable growth advantage, especially at medium to high cell densities. Both findings indicate that elevated IGF2BP1 levels diminish contact inhibition of growth in ES-2 cells. Consistently, high-resolution imaging of 2D-cultured ES-2 cells demonstrated that G-I1 expression promotes multilayered cell growth, a phenomenon only rarely observed in the GFP-expressing control population (Fig. 1E).

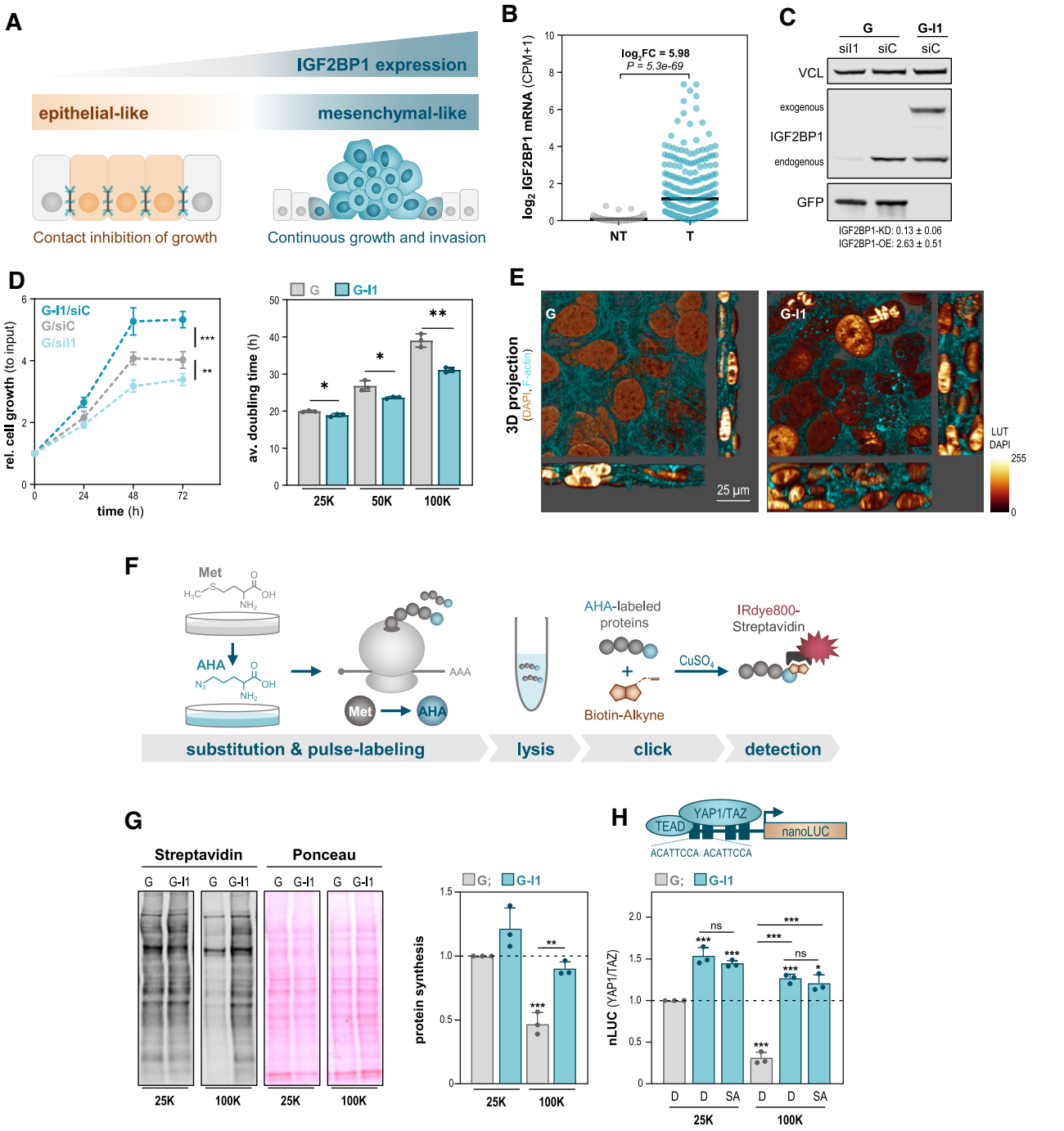

Figure 1. IGF2BP1 prevents contact inhibition of tumor cell growth. (**A**) Schematic of elevated mesenchymal-like invasive growth and reduced contact inhibition by the oncogene IGF2BP1 in carcinomas. (**B**) IGF2BP1 mRNA expression in normal ovarian tissue (NT, GTex v7) versus ovarian cancer (T; TCGA-RNA-seq). (**C**) Western blot of IGF2BP1 knockdown and overexpression in ES-2 cells. VCL served as loading control. Knockdown and overexpression rates are indicated below panel. (**D**) IGF2BP1 impacts 2D cell growth at high cell densities. Growth curve of IGF2BP1 overexpression and knockdown cells (panel C) determined by Cell-Titer-Glo® (left panel). Doubling times over a growth period of 72 h were assessed for different initial seeding densities: 25 000 cells/cm^2 (25K); 50 000 cells/cm^2 (50K); and 100 000 cells/cm^2 (100K). (**E**) IGF2BP1 overexpression impairs the contact inhibition of growth. Representative 3D projections of ES-2 cells overexpressing GFP (G) or GFP–IGF2BP1 (G–I1). Cells were co-labeled by DAPI and Phalloidin at high seeding densities. (**F**) Schematic depicting the labeling of newly synthesized proteins using CLICK-IT™ chemistry. (**G**) IGF2BP1 overexpression promotes protein synthesis at high cell densities. Nascent protein production was monitored by pulse-labeling at indicated conditions using Strepavidin-R800 (left panel) labeling. Ponceau staining served as loading control. Relative protein synthesis (to GFP controls) is represented by a bar diagram (right panel). (**H**) IGF2BP1 overexpression promotes YAP1/TAZ-driven transcription. NanoLuc® activity of transcriptional luciferase reporters (schematic in top panel) harboring four YAP1/TAZ response elements at indicated conditions [SA: Saracatinib at 5 µM; D: DMSO at 0.05% (v/v)] is shown by a bar diagram. Error bars indicate standard deviation (s.d.) of three independent experiments: $*P < 0.05$; $**P < 0.01$; $***P < 0.001$.

One hallmark of contact-induced growth arrest is the downregulation of cap-dependent mRNA translation, which involves an increased abundance of the translational repressor 4E-BP1 and potentially impaired initiation efficacy due to disturbed eIF4A activity [58, 59]. To determine if IGF2BP1 influences protein biosynthesis in a cell density-dependent manner, pulse chase experiments were conducted using the methionine analog AHA. This approach allowed tracing nascent protein production via CLICK chemistry (Fig. 1F). At low cell densities (25 000 cells/cm^2), GFP-IGF2BP1 expression only moderately enhanced protein biosynthesis in ES-2 cells (Fig. 1G). In sharp contrast, elevated IGF2BP1 abundance substantially increased global mRNA translation at high cell densities (four-fold, 100 000 cells/cm^2). This suggests that the significant upregulation of IGF2BP1, observed in advanced malignancies, stimulates cancer hallmark pathways, promoting tumor growth at elevated cell densities. To identify pathways involved in the IGF2BP1-dependent regulation of contact inhibition in ovarian cancer, we investigated IGF2BP1-correlated genes in the ovarian serous cystadenocarcinoma dataset provided by the TCGA ($n = 304$). ORAs identified "cell cycle", "signaling pathways regulating pluripotency of stem cells", and the "Hippo signaling pathway" among the most significantly stimulated pathways associated with IGF2BP1 expression in EOC (Supplementary Fig. S1F). In support of these findings, previous studies reported roles of IGF2BPs in cell cycle control [26], stem-cell fate decisions [60], and their association with the YAP1/TAZ-driven gene expression in glioma and liver cancer [14, 61].

Aiming to explore if IGF2BP1 modulates YAP1/TAZ-driven gene expression in EOC-derived cells, we monitored the activity of YAP1/TAZ-driven transcriptional luciferase reporters in G-I1-expressing ES-2 cells at low and high densities (Fig. 1H and Supplementary Fig. S1G). Notably, elevated IGF2BP1 expression significantly enhanced YAP1/TAZ transcriptional activity by about 1.5-fold at low densities. Consistent with the observed changes in global translation (cf. Fig. 1G), YAP1/TAZ-driven gene expression in control cells was markedly reduced at high cell densities due to contact inhibition (Fig. 1H), a phenomenon not observed with minimal promoter reporters (Supplementary Fig. S1G). In stark contrast, IGF2BP1 overexpression maintained YAP1/TAZ-driven gene expression even under high-density conditions. Given that SRC is known to enhance YAP1/TAZ activity to drive tumor growth and metastasis [43] and IGF2BP1 induces SRC activity in EOC cells [37], we investigated if IGF2BP1-promoted YAP1/TAZ-driven gene expression was SRC-dependent. Interestingly, high levels of YAP/TAZ-driven transcription in IGF2BP1-overexpressing cells persisted despite SRCi by treatment with Saracatinib. This is consistent with previous findings, which show that Saracatinib primarily impairs IGF2BP1-driven invasion, rather than the growth of ovarian cancer cells [37]. Collectively, these results suggest that IGF2BP1 is a potent enhancer of YAP1/TAZ-driven gene expression, promoting tumor growth at high cell density in an SRC-independent manner in ES-2 cells.

IGF2BP1 promotes YAP1 abundance and transcriptional activity in ovarian cancer

The Hippo signaling pathway regulates YAP1/TAZ-driven gene expression through cytoplasmic phosphorylation of YAP1/TAZ, resulting in their cytoplasmic retention, decay, and increased association with AJs [9]. Upon dephosphorylation, YAP1s/TAZs translocate to the nucleus, where they induce target gene expression in conjunction with TEAD transcription factors. This suggests that phosphorylated cytoplasmic and AJ-associated YAP1 aligns with rather tumor-suppressive roles, whereas dephosphorylated nuclear YAP1/TAZ promotes pro-proliferative and tumorigenic gene expression (Fig. 2A).

To identify direct effectors of IGF2BP1-stimulated YAP1/TAZ-driven gene expression in EOC, we examined the correlation of core Hippo pathway genes with IGF2BP1 in patient samples and upon IGF2BP1 knockdown in ES-2 cells (Fig. 2B). We observed positive correlations with IGF2BP1 for all oncogenic but not tumor suppressive core Hippo pathway genes. Moreover, IGF2BP1 expression was associated with enhanced expression of previously described YAP1 target genes (Fig. 2C) [53]. Among oncogenic core Hippo pathway genes, only YAP1 and TEAD4 mRNAs were substantially downregulated upon IGF2BP1 depletion in ES-2 cells. The analysis of IGF2BP1-CLIP data from four cell line models [24] revealed a conserved association between IGF2BP1 and YAP1 mRNA, but not TEAD4 transcripts (Fig. 2B and Supplementary Fig. S2A). These findings suggest that IGF2BP1 stimulates YAP1/TAZ-driven gene expression by directly targeting the YAP1 mRNA.

Two major YAP1 isoforms, YAP1-1 and YAP1-2, arising from alternative splicing and differing in the number of WW domains, have been reported [62]. Consistent with reduced total YAP1 mRNA levels, protein abundance of both isoforms decreased upon IGF2BP1 knockout and knockdown in ES-2 cells (Fig. 2D). Conversely, GFP-IGF2BP1 expression elevated both, YAP1 mRNA and protein levels (Supplementary Fig. S2B). Relative phosphorylation of YAP1 at serine 127, however, remained largely unchanged following IGF2BP1 knockdown (Supplementary Fig. S2C). This indicates that IGF2BP1 does not directly modulate Hippo signaling but instead increases the overall abundance of YAP1.

The functional impact of YAP1 abundance on IGF2BP1-mediated effects was assessed by overexpressing the YAP1-1 isoform, which increased YAP/TAZ-driven luciferase reporter activity and cell growth (Supplementary Fig. S2D). Likewise, the stimulation of both YAP1/TAZ-reporter activity and cell growth by GFP-IGF2BP1 was diminished by YAP1 depletion (Supplementary Fig. S2E). Most notably, impaired growth and YAP1/TAZ-reporter activity upon IGF2BP1 knockdown were restored by the re-expression of YAP1-1 (Fig. 2E). Consistent with our observation of IGF2BP1-stimulated YAP1 expression, GSEA of IGF2BP1-depleted ES-2 cells revealed significant downregulation of YAP1 target genes previously identified by Galli *et al.* [53] (Fig. 2F). In conclusion, these findings demonstrate that IGF2BP1 enhances YAP1/TEAD-driven gene expression by promoting the synthesis of YAP1.

IGF2BP1 elevates YAP1 synthesis in a 3′UTR- and m^{6}A-dependent manner

To delineate the molecular basis of IGF2BP1-mediated regulation of YAP1/TAZ-driven gene expression, we focused on two prime candidate targets: YAP1 and TEAD4 (cf. Fig. 2B). IGF2BP1 binding to YAP1 and TEAD4 mRNAs was determined by RIP studies in ES-2 cells lacking IGF2BP1, and re-expressing either GFP (control), a previously char-

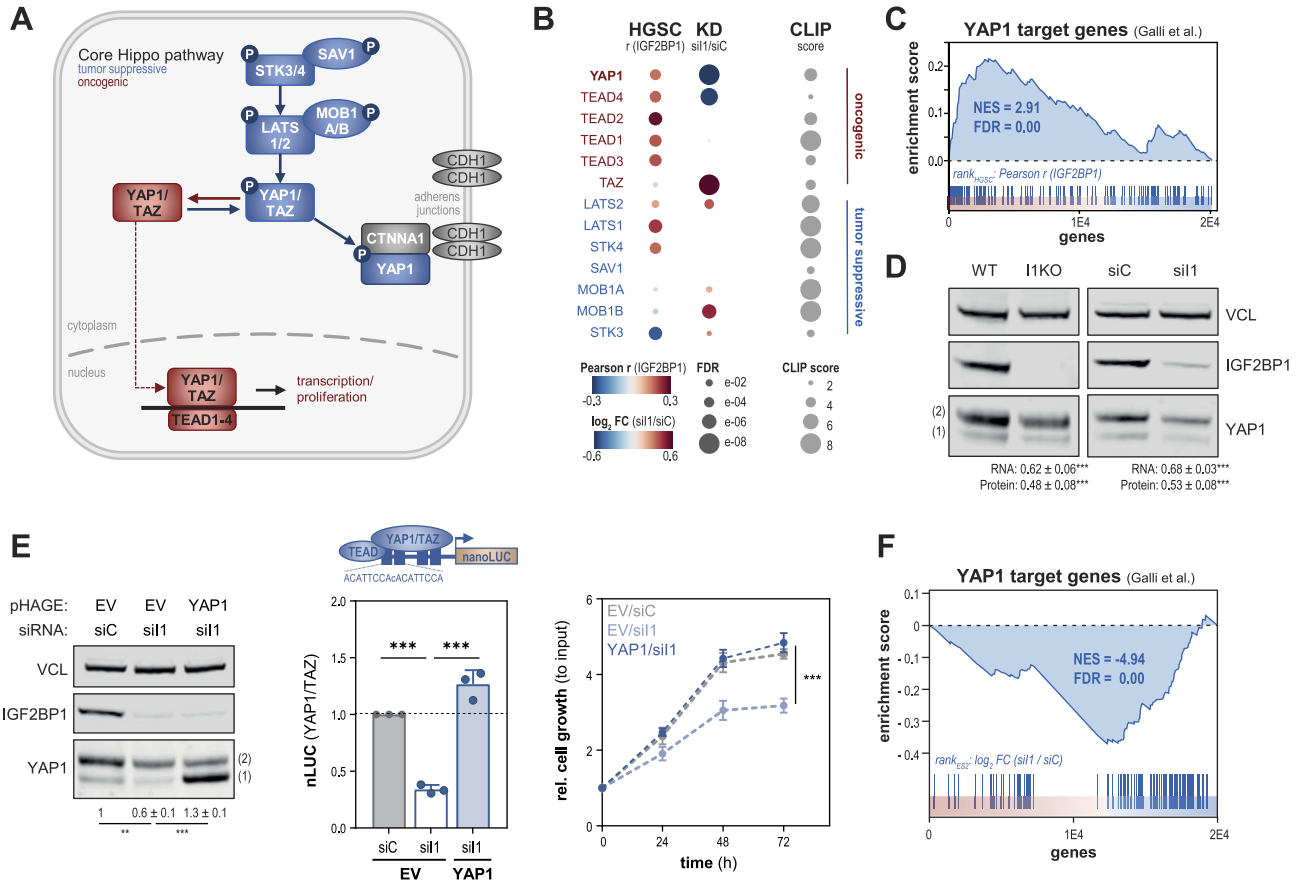

Figure 2. IGF2BP1 promotes tumor cell growth by enhancing YAP1 expression. (**A**) Schematic of the core Hippo signaling pathway. Tumor suppressor genes are indicated in blue, oncogenic factors are shown in red. (**B**) IGF2BP1 is associated with YAP1 and TEAD4 expression in ovarian cancer. For indicated genes, the bubble chart depicts Pearson correlation (r) with IGF2BP1 expression in EOC (TCGA-OV-304), fold changed expression in ES-2 cells upon IGF2BP1 depletion (KD), and IGF2BP1-CLIP scores [24]. (**C**) IGF2BP1 is associated with elevated YAP1-driven target gene expression. GSEA upon gene ranking according to IGF2BP1 Pearson correlation with IGF2BP1 (TCGA-OV-304 dataset). The enrichment plot for YAP1 target genes by Galli *et al.* [53] is shown. (**D**) IGF2BP1 promotes YAP1 synthesis. Western blot analysis of CRISPR/Cas9-based IGF2BP1 knockout (I1KO) or IGF2BP1 depletion by an siRNA pool (sil1). Distinct YAP1 isoforms, YAP1-1 [1] and YAP1-2 [2], are highlighted. Protein and RNA quantifications are provided below panels. (**E**) YAP1 re-expression rescues growth and YAP1/TAZ reporter activity upon IGF2BP1 depletion. Western blot analysis of indicated proteins (left panel), NanoLuc® activity of transcriptional YAP1/TAZ reporters (middle panel), and 2D growth of ES-2 cells (right panel) were determined for controls (siC/EV), IGF2BP1-depletion (sil1), and YAP1 re-expression upon IGF2BP1 knockdown (YAP1/sil1). (**F**) IGF2BP1 depletion impairs YAP1-driven gene expression. GSEA for the YAP1 target gene set by Galli *et al.* [53] upon gene ranking by the fold change of expression in response to IGF2BP1 depletion in ES-2 cells. Error bars indicate s.d. of three independent experiments: $*P < 0.05$; $**P < 0.01$; $***P < 0.001$.

acterized RNA-binding deficient IGF2BP1-mutant (KH) [37, 63], or the GFP-fused wild-type IGF2BP1 (G-I1; Fig. 3A). Only the wild-type protein co-purified with ELAVL1 (HuR), a previously reported RNA-dependent binding partner of IGF2BP1 [64] (Supplementary Fig. S3A). RIP studies indicated strong enrichment of YAP1 and the previously reported, conserved target mRNA HMGA2 [23]. In sharp contrast, and consistent with the lack of conserved CLIP hits for IGF2BP1 (cf. Supplementary Fig. S2A), TEAD4 transcripts were not enriched with G-I1 above control levels. To corroborate direct association of IGF2BP1 with the YAP1 mRNA, we focused on a high-confidence binding site identified by eCLIP studies in HEPG2 cells [21]. This site overlaps with reported miRNA-binding sites for the miR-16 family, known to regulate YAP1 expression in gastric- and cholangiocarcinoma [13, 65] (Supplementary Fig. S2A). Isothermal spectral shift spectroscopy analyses and MST with recombinant human IGF2BP1 and a Cy5-labeled RNA probe derived from the YAP1 high-confidence binding site confirmed robust binding with K_d values in the low nanomolar range (Supplementary Fig. S3B). Further validation using RIP studies showed that BTYNB (BT) significantly reduced IGF2BP1's association with both HMGA2 and YAP1 mRNAs (Supplementary Fig. S3C). In view of IGF2BP1's conserved role in stabilizing mRNAs in cancer cells [21], these findings strongly suggested RNA-binding-dependent enhancement of YAP1 expression by IGF2BP1.

In support, only the re-expression of wild-type IGF2BP1, but not the RNA-binding deficient mutant (KH) restored YAP1 expression in IGF2BP1-knockout ES-2 cells (Fig. 3B). The hypothesis that IGF2BP1 stabilizes YAP1 mRNA was tested by RNA decay assays following transcriptional inhibition via Actinomycin D (Fig. 3C). These studies demonstrated ~3-fold increase in YAP1 mRNA degradation in IGF2BP1-deleted ES-2 cells, confirming IGF2BP1's role in stabilizing YAP1 mRNA. The investigation of reported IGF2BP1-CLIP sites in the YAP1 mRNA suggested strong association at the 3′UTR and thus 3′UTR-dependent regulation (cf. Supplementary Fig. S2A), as previously reported for various target mRNAs stabilized by IGF2BP1 [21, 24–26]. Luciferase

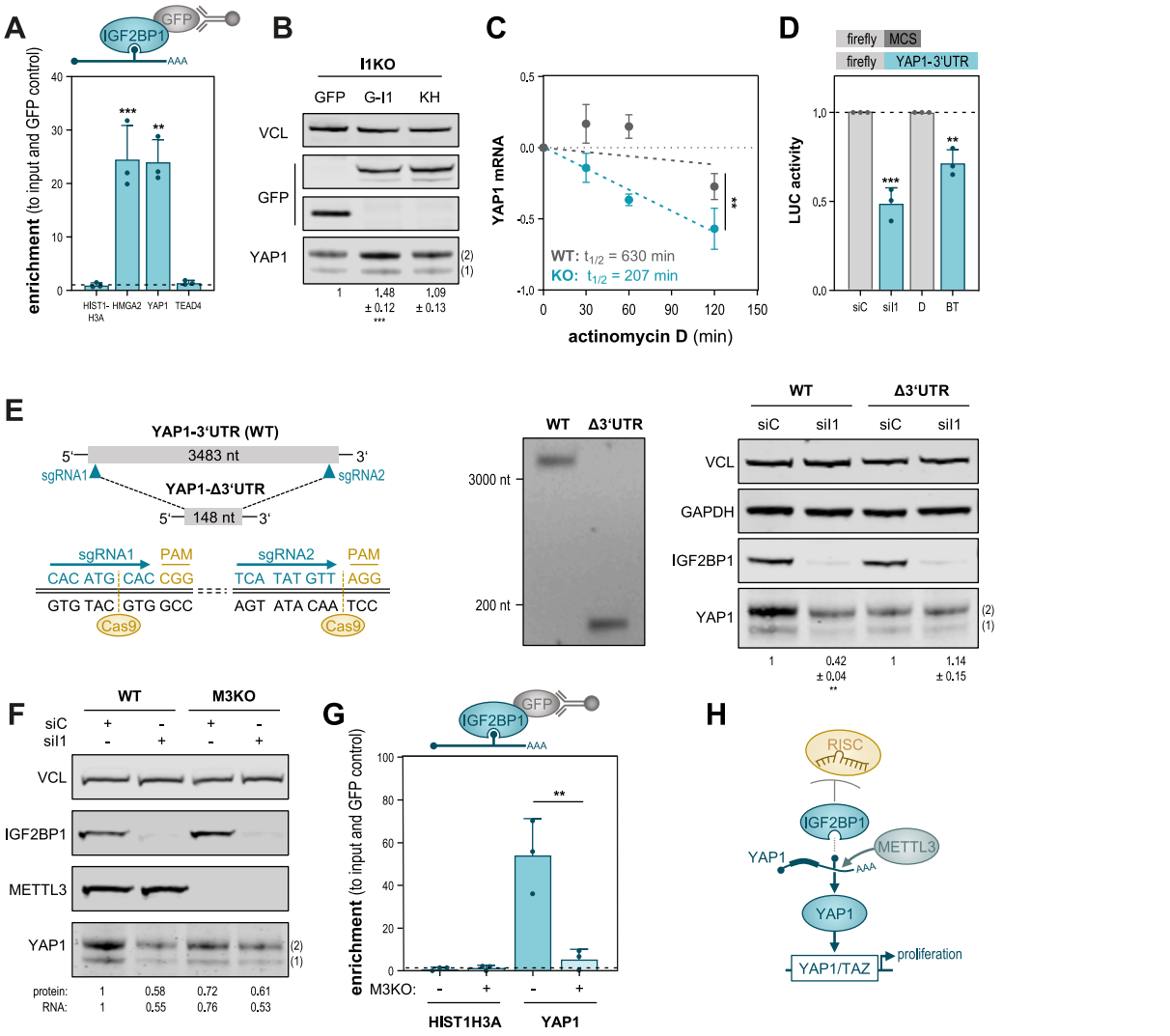

Figure 3. IGF2BP1 is an m^{6}A-/3′UTR-dependent enhancer of YAP1 mRNA stability. (**A**) IGF2BP1 associates with the YAP1 mRNA. IGF2BP1-RIP analyses in IGF2BP1-knockout (I1-KO) ES-2 cells re-expressing GFP (control), RNA-binding deficient GFP-IGF2BP1 (control), or GFP-IGF2BP1. RNA enrichment was normalized to inputs and the GFP control. Pulldown controls are shown in Supplementary Fig. S3A. (**B**) RNA-dependent enhancement of YAP1 by IGF2BP1. Western blot analysis in I1-KO ES-2 cells re-expressing GFP (control), GFP-IGF2BP1 (G-I1), or RNA-binding deficient IGF2BP1 (KH). Protein quantification is depicted in lower panel. (**C**) IGF2BP1 stabilizes the YAP1 mRNA. RNA turnover analyses in parental ES-2 (WT) and I1-KO cells (KO) following Actinomycin D treatment at indicated timepoints. (**D**) IGF2BP1 controls YAP1 expression in a 3′UTR-dependent manner. Changes in the activity of luciferase reporters containing the YAP1-3′UTR were determined in ES-2 cells depleted for IGF2BP1 (sil1) or exposed to BTYNB (10 μM). (**E**) Deletion of the YAP1-3′UTR abolishes regulation by IGF2BP1. The schematic (left panel) shows the strategy of 3′UTR-deletion, as verified by PCR (middle panel). Western blot analysis of YAP1 protein expression (right panel, quantification in lower panel) upon IGF2BP1 depletion in parental (WT) and 3′UTR-deleted ES-2 cells (Δ3′UTR). (**F**) Modification by m^{6}A promotes IGF2BP1-stimulated YAP1 expression. Western blot analysis of indicated proteins in parental (WT) and METTL3-deleted (M3KO) ES-2 cells upon IGF2BP1 depletion. Protein and mRNA quantification are shown below panel. (**G**) Modification by m^{6}A promotes association of IGF2BP1 with the YAP1 mRNA. IGF2BP1-RIP analysis in parental and M3KO ES-2 cells stably expressing GFP-IGF2BP1 or GFP as control. RNA enrichments were normalized to inputs and the GFP control. Pulldown controls are shown in Supplementary Fig. S3F. (**H**) Schematic of IGF2BP1-directed, m^{6}A and 3′UTR-dependent enhancement of YAP1 mRNA stability. Error bars indicate s.d. of three independent experiments: $^{**}P < 0.01$; $^{***}P < 0.001$.

reporters containing the YAP1 3′UTR showed ~2-fold reduced activity following IGF2BP1 knockdown and, most notably, in response to BTYNB treatment (Fig. 3D). The critical role of the 3′UTR was further corroborated by CRISPR-guided deletion of the YAP1-3′UTR. This significantly reduced YAP1 protein abundance and abolished IGF2BP1-dependent regulation (Fig. 3E). Studies in glioma cell models suggested that IGF2BP1 controls YAP1 abundance in an m^{6}A-dependent manner [14]. Consistent with this, YAP1 mRNA harbors several m^{6}A sites (Supplementary Fig. S2A) according to RMBase [46, 47]. Deletion of the m^{6}A methyltransferase METTL3 in ES-2 cells reduced global m^{6}A levels, YAP1 expression, and cell growth, whereas IGF2BP1 abundance remained essentially unaffected (Fig. 3F and Supplementary Fig. S3D–F). Notably, IGF2BP1 knockdown still modestly reduced YAP1 levels in METTL3-deficient cells, suggesting that m^{6}A modification promotes, but is not essential for, the IGF2BP1-mediated regulation of YAP1. In agreement with a stimulatory role of m^{6}A modification, RIP studies showed diminished YAP1 mRNA association with IGF2BP1 in METTL3-deleted cells

(Fig. 3G, and Supplementary Fig. S3F). In summary, these findings establish IGF2BP1 as a druggable regulator of YAP1 abundance, functioning through a combination of m^{6}A- and 3′UTR-dependent mechanisms (Fig. 3H).

IGF2BP1 is a druggable enhancer of YAP1-driven gene expression in carcinomas

To investigate if IGF2BP1 and YAP1 are co-expressed in ovarian cancer samples, a TMA containing 35 primary HGSC samples with corresponding metastases of the greater omentum was used for multispectral imaging (Fig. 4A). To this end, multicolor fluorescence counter staining of YAP1, IGF2BP1, and pan-CK to distinguish tumor from stroma tissue, and DAPI labeling to reveal nuclei was employed. Quantification of cytoplasmic IGF2BP1 signals significantly correlated with nuclear YAP1 staining in tumor cells. This suggests that IGF2BP1 promotes YAP1 abundance and activity in ovarian cancer, as indicated by enriched nuclear localization of the protein in IGF2BP1-expressing cancer cells.

IGF2BP1 is a conserved pro-tumorigenic factor in carcinomas, which is druggable by BTYNB resulting in significant downregulation of pro-proliferative cancer hallmark pathways, e.g. E2F- and MYC/MYCN-driven gene expression [17, 26]. To evaluate if this is also observed for YAP1-driven transcription, we explored the association of IGF2BP1 with YAP1/TAZ target gene sets in TCGA-provided gene expression data of five carcinomas (LUAD, HNSC, OV, LIHC, and PAAD) with reported oncogenic roles of IGF2BP1 [26, 66]. To this end, correlation coefficients determined for IGF2BP1-associated gene expression were used for gene ranking and subsequent GSEA (Fig. 4B). These analyses indicated that IGF2BP1 is significantly associated with enhanced YAP1/TAZ gene expression in all five investigated carcinomas. This was most consistent for the YAP1 target gene set reported by Galli *et al.* [53], for which the highest normalized enrichment scores (NESs) were determined except for HNSC. If IGF2BP1 controls YAP1 expression in a conserved manner, was addressed by monitoring the expression of Hippo pathway genes upon IGF2BP1 knockdown (Fig. 4C and D). RNA-seq data derived from five cell lines revealed a quite heterogeneous deregulation of Hippo pathway genes across investigated cell models upon IGF2BP1 depletion, with YAP1 being a striking exception (Fig. 4C). In response to IGF2BP1 knockdown, only the YAP1 mRNA showed consistently decreased abundance in all investigated cell models, although downregulation remained moderate in SAS (HNSC) cells. However, at the protein level, IGF2BP1 significantly decreased YAP1 protein abundance in all tested cell lines (Fig. 4D). This decrease of YAP1 was associated with significantly reduced expression of YAP1 target genes reported by Galli *et al.* [53] (Fig. 4E). Consistent with a conserved impact on cell vitality (Supplementary Fig. S4A), BTYNB induced robust downregulation of YAP1 expression in all cell models exposed to BTYNB at EC_{50} concentrations for 72 h (Fig. 4F). Whether the inhibition of IGF2BP1–RNA association by BTYNB also impairs YAP1/TAZ-driven gene expression was investigated by transcriptional luciferase reporters in all investigated cell models (Fig. 4G). In line with the demonstrated, conserved reduction of YAP1 expression and cell proliferation, BTYNB significantly reduced YAP1/TAZ-reporter activity in all tested cell lines. In summary, these findings demonstrate that IGF2BP1 is a conserved enhancer of YAP1 expression and YAP1/TAZ transcriptional activity. This stimulatory role is substantially disrupted by BTYNB, which interferes with IGF2BP1–RNA association (Fig. 4H).

IGF2BP1i provides versatile therapeutic benefits by impairing invasive tumor growth

In previous studies, we demonstrated that IGF2BP1 promotes the invasive growth of ovarian cancer cell models [37]. Consistent with these findings, the IGF2BP1 inhibitor BTYNB impaired both 3D growth and spheroid invasion of ovarian cancer derived ES-2 cells (Fig. 5A and B). The growth-inhibitory effect of BTYNB was strikingly conserved with EC_{50} values in the low micromolar range, as determined in five 2D-cultured tumor cell models (Supplementary Fig. S4A). In sharp contrast, SRCi by Saracatinib only showed strong inhibition of 2D growth in A549 and SAS cells ($EC_{50} < 1$ μM), whereas it remained substantially less effective in ES-2, HUH-7, and PANC-1 cells where EC_{50} values ranged between ∼10 and 600 μM. These observations suggested that Saracatinib's impact on cell viability is at least partially mediated through its inhibition of YAP1/TAZ-driven gene expression. Supporting this notion, we found that A549 and SAS cells exhibited lower YAP1 expression relative to SRC, while HUH-7, ES-2, and PANC-1 cells had higher YAP1/SRC expression ratios (Fig. 5C and Supplementary Fig. S4B). To test this hypothesis, we monitored the transcriptional activity of YAP1/TAZ-luciferase reporters in response to Saracatinib (Fig. 5D). Unlike BTYNB, which uniformly inhibited reporter activity and cell viability across all cell models tested (cf. Fig. 4G), Saracatinib reduced reporter activity predominantly in A549 and SAS cells. This suggests that SRCi impairs cell viability, at least in part, by suppressing YAP1/TAZ-driven gene expression in Saracatinib-sensitive cell models. The broad inhibitory effect of targeting YAP1/TAZ signaling on cell proliferation was confirmed using Verteporfin, an indirect YAP1/TAZ inhibitor (Supplementary Fig. S4B).

These findings prompted us to hypothesize that Verteporfin enhances the potency of SRCi, at least in cell models with high YAP1/SRC ratios and low Saracatinib response. Supporting this notion, combined treatment with Saracatinib and Verteporfin produced only moderate additive effects in A549 cells, as determined by the HSA model [44, 45] (Fig. 5E). In contrast, synergistic effects were observed in ES-2 cells, with delta scores exceeding 10 (Fig. 5E). Consistent with the direct regulation of SRC and YAP1 by IGF2BP1, the combined treatment of ES-2 cells with BTYNB and either Saracatinib or Verteporfin demonstrated substantial additivity, with average delta scores between 0 and 10 (Supplementary Fig. S4C).

Overall, these findings highlighted a crucial role of IGF2BP1 which promotes both, SRC [37] and YAP1/TAZ activity in a conserved manner across carcinomas. Thus, we hypothesized that concurrent inhibition of IGF2BP1 (BTYNB), SRC (Saracatinib), and YAP1/TAZ (Verteporfin) provides robust inhibition of both growth and invasion in ovarian cancer and other carcinomas. This hypothesis was tested using 3D-invasion assays on ES-2 cells and organoid growth assays on EOC tumor organoids. Both models express all three proteins at variable abundances and were responsive to high dose single-agent treatments (Fig. 5F and Supplementary Fig. S4D). The combination of all three inhibitors significantly impaired spheroid invasion and organoid growth (Fig. 5G)

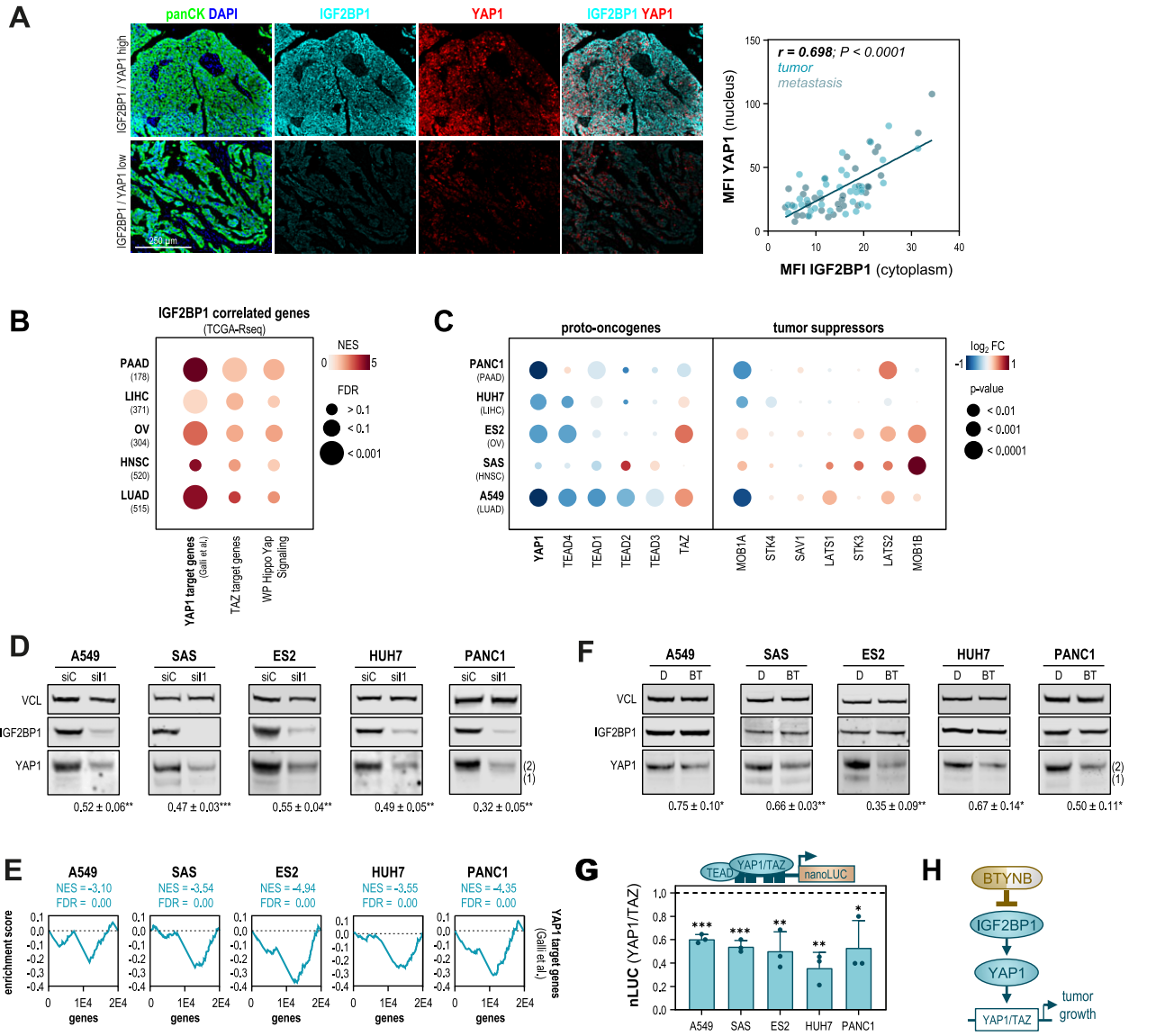

Figure 4. IGF2BP1 is a conserved enhancer of YAP1 and its target genes in carcinomas. (**A**) IGF2BP1 expression is associated with elevated nuclear YAP1 abundance in ovarian cancer. Co-expression of IGF2BP1 and YAP1 was monitored by multicolor fluorescence imaging on a TMA comprising 35 HGSC samples and corresponding metastases in the greater omentum. Representative images (left panel) show protein expression (IGF2BP1 and YAP1) next to representative labeling of nuclei by DAPI and tumor cells by pan-CK staining. Pearson correlation of mean fluorescence intensities per core identified a significant co-expression of IGF2BP1 and YAP1, as depicted by an XY plot (right panel). (**B**) IGF2BP1 shows conserved association with YAP1/TAZ target gene expression in carcinomas. Bubble plots indicate NESs determined by GSEA of IGF2BP1-correlated gene expression (Pearson) in five carcinomas-based TCGA-deposited RNA-seq datasets. (**C**) IGF2BP1 is a conserved regulator of YAP1 expression in carcinoma cells. Bubble plots show the fold change in gene expression of core Hippo pathway genes, as determined upon IGF2BP1 depletion in tumor cell lines derived from indicated carcinomas. (**D**) IGF2BP1 depletion consistently impairs YAP1 expression in carcinoma-derived cell lines. Western blot analysis of IGF2BP1 and YAP1 upon I1-KD in indicated cell lines. Changes in YAP1 protein abundance are shown in the lower panels. (**E**) IGF2BP1 is a conserved enhancer of YAP1 target genes. GSEA by ranking genes in response to IGF2BP1 depletion identifies consistent downregulation of YAP1 target genes reported by Galli *et al.* [53] in five carcinoma-derived cell lines. (**F**) Inhibition of IGF2BP1 by BTYNB consistently reduces YAP1. Western blot analysis of IGF2BP1 and YAP1 in response to BTYNB (10 µM) in indicated cell lines. Changes in YAP1 protein abundance are shown in the lower panels. (**G**) BTYNB is a conserved inhibitor of YAP1/TAZ-driven transcription. NanoLuc® activity of transcriptional reporters comprising four YAP1/TAZ binding elements (schematic in upper panel) was monitored upon exposure to BTYNB (10 µM) in indicated cell lines. (**H**) The schematic illustrates inhibition of the IGF2BP1–YAP1 axis by BTYNB. Error bars indicate s.d. of three independent experiments: $*P < 0.05$; $**P < 0.01$; $***P < 0.001$.

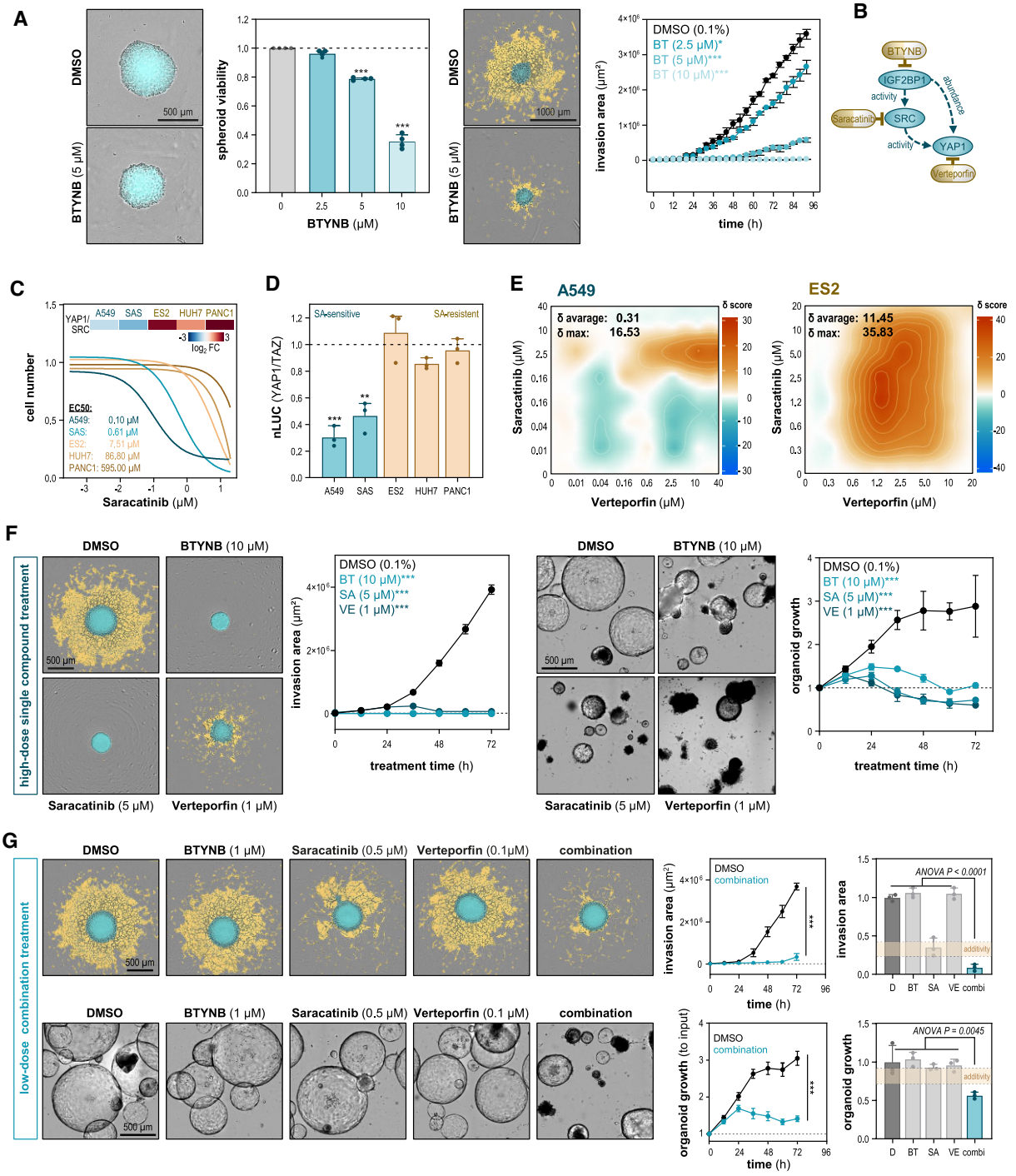

Figure 5. IGF2BP1i provides conserved benefits in sensitizing carcinoma cells to SRCi and combined treatment with YAP1/TAZ inhibition. (**A**) IGF2BP1i by BTYNB impairs 3D growth and 3D invasion in ES-2 cells. Spheroid growth (left panel) and invasion (right panel) of ES-2 was evaluated upon BTYNB exposure at indicated concentrations for 72 h. The spheroid body is highlighted in turquoise. The invasive area is indicated in yellow. The quantitative assessment of spheroid viability, determined by Cell-Titer Glo®, and invasion areas are depicted by a bar diagram (left panel) and XY plots (right panel). (**B**) Schematic illustrating the impairment of YAP1-driven gene expression by IGF2BP1i (BTYNB), SRCi (Saracatinib), and YAP1/TAZi (Verteporfin). (**C**) Low potency of SRCi is associated with elevated YAP1/SRC abundancy ratios. Dose-response curves of SRCi for indicated cell lines. EC_{50}-values are indicated. Heatmap shows $\log_2$ YAP1/SRC mRNA ratios, as determined by RNA-seq, for respective cell lines. (**D**) Resistance to SRCi is associated with transcriptional YAP1/TAZ activity. NanoLuc® activity of transcriptional YAP1/TAZ luciferase reporters was monitored in SRCi responsive (turquoise) and resistant (yellow) cell lines. DMSO served as control. (**E**) SRCi shows strong synergy with YAP1/TAZi in SRCi-resistant cell models. Images depict synergy maps derived by Saracatinib versus Verteporfin drug combination matrices and evaluation by the HSA model [45] for indicated cell lines. Synergy: $10 < \delta$ (delta score) < 100; additivity: $0 < \delta < 10$; antagonism: $\delta < -10$. (**F, G**) Combined IGF2BP1i, SRCi, and YAP1/TAZi provides robust and conserved impairment of invasive growth in cell line models and organoids. Invasion and organoid growth were assessed 72 h upon exposure to mono- or combination treatments at indicated concentrations of individual compounds. Representative images are shown. Changes relative to the starting point of the treatment are shown as line plots for indicated conditions. Bar diagrams depict changes relative to DMSO controls (panel G; right panels). Additivity, defined as the summed effects of all compounds, is highlighted in yellow. Error bars indicate standard errors of the mean of three independent experiments: $^*P < 0.05$; $^{***}P < 0.001$.

using doses ~10-fold lower in the triple-treatment regimen compared with those effective in monotherapies (cf. Fig. 5F). Furthermore, the triple treatment exhibited synergistic effects, as low-dose single-agent treatments had minimal impact, except for Saracatinib, which partially reduced invasion (Fig. 5G).

In conclusion, these findings highlight a strongly conserved potential of IGF2BP1i by BTYNB on YAP1/TAZ-driven growth and SRC-dependent invasion. The regulatory crosstalk among IGF2BP1, SRC, and YAP1 further indicates combined treatment regimens as a promising approach to achieve robust responses at low dosages of individual compounds.

Discussion

Our study provides compelling evidence that IGF2BP1 plays a multifaceted role in promoting tumor growth [20], both by enhancing cellular proliferation and impairing contact inhibition of growth. This dual function further highlights IGF2BP1 as a critical oncogenic driver across various carcinoma models [24, 26], extending its established oncogenic role in neuroblastoma and other malignancies [17, 29, 30]. Importantly, our findings for the first time reveal that IGF2BP1's conserved regulatory effects largely rely on the upregulation of YAP1. This key effector of the Hippo signaling pathway serves essential roles in tumorigenesis, particularly in regulating contact inhibition of growth [5]. Building on previous research in glioma [14], our work shows that IGF2BP1 promotes YAP1 expression by stabilizing the YAP1 mRNA through an m^{6}A- and YAP1-3′UTR-dependent mechanism. This discovery underscores the importance of RNA modifications in cancer biology [27], particularly the role of m^{6}A in enhancing IGF2BP1's ability to bind and stabilize some of its target mRNAs [21], as previously shown for other oncogenic factors like MYC and SRF [18, 25]. The critical nature of the YAP1 3′UTR in this process is confirmed by our observation that deleting this regulatory *cis*-element abolishes IGF2BP1-directed control of YAP1 expression. In line with a supportive role of m^{6}A in IGF2BP1-stimulated YAP1 expression, we observed that deletion of METTL3 reduces YAP1 abundance attenuating IGF2BP1-directed stimulation. However, the direct recognition of m^{6}A by IGF2BP1 remains a topic of debate, and further work is needed to elucidate the molecular details how m^{6}A contributes to IGF2BP1-mediated YAP1 regulation. Nevertheless, our findings indicate that m^{6}A modifications are not required but support the stabilization of YAP1 mRNA mediated by IGF2BP1, aligning with previous reports on other oncogenes such as MYC and SRF [18, 25].

A pivotal aspect of our study is the identification of BTYNB's potency in disrupting IGF2BP1–YAP1 mRNA association, as has been shown for other IGF2BP1 target transcripts [17, 26, 31]. This inhibitory potential manifests in the conserved impairment of 3D growth and invasion in ovarian cancer cells and organoids. Here, we, for the first time, demonstrate that this is intimately linked to BTYNB's impact on YAP1-driven transcriptional activity. Significantly, BTYNB's potency is enhanced when combined with Verteporfin, an indirect YAP1/TAZ inhibitor elevating 14-3-3 proteins to sequester YAP1 in the cytoplasm [10]. Consistent with previous reports we also observed benefits of combining BTYNB with SRCi using Saracatinib [37]. These findings emphasize the broad therapeutic potential of IGF2BP1 targeting, which affects multiple pathways in concert, including the oncogenic activation of SRC [43], which appears limited in mesenchymal-like carcinoma cells like ES-2. In these, inhibitors like BTYNB and Verteporfin overcome these limitations of Saracatinib through diminishing growth and acting in synergy with SRCi. In contrast, in rather epithelial-like cells like A549 or SAS, which maintain CDH1-positive AJs, SRCi strongly impacts on tumor cell growth with limited benefits observed in combined treatment. These findings are concise with the notion that YAP1 activity is likely restricted due to its tight recruitment to AJs via α-catenin [67] and elevated activity of the YAP1 repressor LATS1 [68]. In mesenchymal cells, lacking AJs like ES-2 cells [37], SRCi likely remains less effective in growth control since repression of YAP1 activity via AJ-based cytoplasmic retention is rendered largely irrelevant [69]. Thus, IGF2BP1 inhibition is superior since it uncouples both, SRC and YAP1 activation from canonical signaling. In the case of SRC, IGF2BP1 promotes activation independent of upstream signaling via direct protein–ligand binding [37]. Likewise, IGF2BP1 uncouples YAP1 activation from canonical Hippo signaling [70], which typically regulates YAP1 protein turnover and prevents nuclear accumulation. Treatment with Verteporfin, and even more interestingly exposure to BTYNB, prevents this oncogenic activation of YAP1/TAZ-dependent transcription in a conserved manner. These findings highlight a novel vulnerability in targeting YAP1-driven tumor growth and emphasize the super-enhancer role of the oncogene IGF2BP1 in fostering hallmark transcription networks in cancer. By uncoupling multiple potent oncogenic pathways from repressive signaling, including E2F- [26], MYC/MYCN- [17, 18], SRF- [25], and the here reported YAP1-driven gene synthesis, IGF2BP1 promotes the activity of the respective transcription networks by directly enhancing the abundance of transcriptional regulators. This provides a conserved and significant Achilles' heel for therapeutic intervention targetable through a single RNA-binding protein, IGF2BP1. This appears feasible in view of inhibitors like BTYNB and the recent development of additional inhibitory small molecule targeting this RNA-binding protein [31, 34–36]. In conclusion, our study provides a strong rationale to further explore avenues for improving the inhibition of IGF2BP1, which provides a promising strategy for impairing oncogenic YAP1 activity in the treatment of various malignancies.

Acknowledgements

The authors thank the Core Facility Imaging (CFI) and Core Unit for NGS analyses of the Martin Luther University (MLU) for broad support with image and NGS data analysis. We thank Dr Monika Hämmerle, Institute of Pathology of the Martin Luther University (MLU), for kindly providing pHAGE and pHAGE-YAP1 plasmids.

Author contributions: A.S., S.H., and N.B. did the conceptualization of the studies. A.S., N.B, T.S., S.M., A.R., B.B., H.E., M.D., L.M.P., S.T., F.M., R.R., M.L., E.G., and A.H. did the investigations by performing the experimental studies. M.G., D.M., A.S. and N.B. performed the formal analyses of the data including sequencing data. W.S., M.V., and M.W. supervised the experimental design and data interpretation. S.H., N.B. and W.S. aquired funding. N.B. and S.H. conceived the experimental design and wrote the manuscript.

Supplementary data

Supplementary data is available at NAR Cancer online.

Conflict of interest

None declared.

Funding

DFG (FOR5433 and 468534282 to N.B., S.H., and W.S.). DFG (GRK2751 and 449501615 to N.B. and S.H.). Funding to pay the Open Access publication charges for this article was provided by Budget of the institution.

Data availability

RNA sequencing data are deposited on GEO: GSE109605, GSE116136 and GSE283587.

References

1. Arter ZL, Desmond D, Berenberg JL *et al.* Epithelial ovarian cancer survival by race and ethnicity in an equal-access healthcare population. *Br J Cancer* 2024;**130**:108–13. https://doi.org/10.1038/s41416-023-02471-z
2. Ledermann JA, Matias-Guiu X, Amant F *et al.* ESGO-ESMO-ESP consensus conference recommendations on ovarian cancer: pathology and molecular biology and early, advanced and recurrent disease. *Ann Oncol* 2024;**35**:248–66. https://doi.org/10.1016/j.annonc.2023.11.015
3. Clark KL, George JW, Przygrodzka E *et al.* Hippo signaling in the ovary: emerging roles in development, fertility, and disease. *Endocr Rev* 2022;**43**:1074–96. https://doi.org/10.1210/endrev/bnac013
4. Wang D, He J, Dong J *et al.* The HIPPO pathway in gynecological malignancies. *Am J Cancer Res* 2020;**10**:610–29.
5. Gumbiner BM, Kim NG. The Hippo-YAP signaling pathway and contact inhibition of growth. *J Cell Sci* 2014;**127**:709–17. https://doi.org/10.1242/jcs.140103
6. Pavel M, Park SJ, Frake RA *et al.* α-Catenin levels determine direction of YAP/TAZ response to autophagy perturbation. *Nat Commun* 2021;**12**:1703. https://doi.org/10.1038/s41467-021-21882-1
7. Jia Y, Li HY, Wang J *et al.* Phosphorylation of 14-3-3zeta links YAP transcriptional activation to hypoxic glycolysis for tumorigenesis. *Oncogenesis* 2019;**8**:31. https://doi.org/10.1038/s41389-019-0143-1
8. Zanconato F, Cordenonsi M, Piccolo S. YAP/TAZ at the roots of cancer. *Cancer Cell* 2016;**29**:783–803. https://doi.org/10.1016/j.ccell.2016.05.005
9. Piccolo S, Panciera T, Contessotto P *et al.* YAP/TAZ as master regulators in cancer: modulation, function and therapeutic approaches. *Nat Cancer* 2023;**4**:9–26.
10. Wang C, Zhu X, Feng W *et al.* Verteporfin inhibits YAP function through up-regulating 14-3-3sigma sequestering YAP in the cytoplasm. *Am J Cancer Res* 2016;**6**:27–37.
11. Wei C, Li X. The role of photoactivated and non-photoactivated Verteporfin on tumor. *Front Pharmacol* 2020;**11**:557429. https://doi.org/10.3389/fphar.2020.557429
12. Li L, Li R, Wang Y. Identification of small-molecule YAP-TEAD inhibitors by high-throughput docking for the treatment of colorectal cancer. *Bioorg Chem* 2022;**122**:105707. https://doi.org/10.1016/j.bioorg.2022.105707
13. Kang W, Tong JH, Lung RW *et al.* Targeting of YAP1 by microRNA-15a and microRNA-16-1 exerts tumor suppressor function in gastric adenocarcinoma. *Mol Cancer* 2015;**14**:52. https://doi.org/10.1186/s12943-015-0323-3
14. Yang J, Wu X, Wang J *et al.* Feedforward loop between IMP1 and YAP/TAZ promotes tumorigenesis and malignant progression in glioblastoma. *Cancer Sci* 2023;**114**:2053–62. https://doi.org/10.1111/cas.15636
15. Haase J, Misiak D, Bauer M *et al.* IGF2BP1 is the first positive marker for anaplastic thyroid carcinoma diagnosis. *Mod Pathol* 2021;**34**:32–41. https://doi.org/10.1038/s41379-020-0630-0
16. Bell JL, Turlapati R, Liu T *et al.* IGF2BP1 harbors prognostic significance by gene gain and diverse expression in neuroblastoma. *J Clin Oncol* 2015;**33**:1285–93. https://doi.org/10.1200/JCO.2014.55.9880
17. Hagemann S, Misiak D, Bell JL *et al.* IGF2BP1 induces neuroblastoma via a druggable feedforward loop with MYCN promoting 17q oncogene expression. *Mol Cancer* 2023;**22**:88. https://doi.org/10.1186/s12943-023-01792-0
18. Huang H, Weng H, Sun W *et al.* Recognition of RNA N(6)-methyladenosine by IGF2BP proteins enhances mRNA stability and translation. *Nat Cell Biol* 2018;**20**:285–95. https://doi.org/10.1038/s41556-018-0045-z
19. Kobel M, Weidensdorfer D, Reinke C *et al.* Expression of the RNA-binding protein IMP1 correlates with poor prognosis in ovarian carcinoma. *Oncogene* 2007;**26**:7584–9. https://doi.org/10.1038/sj.onc.1210563
20. Bell JL, Wachter K, Muhleck B *et al.* Insulin-like growth factor 2 mRNA-binding proteins (IGF2BPs): post-transcriptional drivers of cancer progression? *Cell Mol Life Sci* 2013;**70**:2657–75.https://doi.org/10.1007/s00018-012-1186-z
21. Glass M, Misiak D, Bley N *et al.* IGF2BP1, a conserved regulator of RNA turnover in cancer. *Front Mol Biosci* 2021;**8**:632219. https://doi.org/10.3389/fmolb.2021.632219
22. Noubissi FK, Elcheva I, Bhatia N *et al.* CRD-BP mediates stabilization of betaTrCP1 and c-myc mRNA in response to beta-catenin signalling. *Nature* 2006;**441**:898–901. https://doi.org/10.1038/nature04839
23. Busch B, Bley N, Muller S *et al.* The oncogenic triangle of HMGA2, LIN28B and IGF2BP1 antagonizes tumor-suppressive actions of the let-7 family. *Nucleic Acids Res* 2016;**44**:3845–64. https://doi.org/10.1093/nar/gkw099
24. Muller S, Bley N, Glass M *et al.* IGF2BP1 enhances an aggressive tumor cell phenotype by impairing miRNA-directed downregulation of oncogenic factors. *Nucleic Acids Res* 2018;**46**:6285–303. https://doi.org/10.1093/nar/gky229
25. Muller S, Glass M, Singh AK *et al.* IGF2BP1 promotes SRF-dependent transcription in cancer in a m^6A- and miRNA-dependent manner. *Nucleic Acids Res* 2019;**47**:375–90. https://doi.org/10.1093/nar/gky1012
26. Muller S, Bley N, Busch B *et al.* The oncofetal RNA-binding protein IGF2BP1 is a druggable, post-transcriptional super-enhancer of E2F-driven gene expression in cancer. *Nucleic Acids Res* 2020;**48**:8576–90. https://doi.org/10.1093/nar/gkaa653
27. Lan Q, Liu PY, Bell JL *et al.* The emerging roles of RNA m(6)A methylation and demethylation as critical regulators of tumorigenesis, drug sensitivity, and resistance. *Cancer Res* 2021;**81**:3431–40. https://doi.org/10.1158/0008-5472.CAN-20-4107
28. Zirkel A, Lederer M, Stohr N *et al.* IGF2BP1 promotes mesenchymal cell properties and migration of tumor-derived cells by enhancing the expression of LEF1 and SNAI2 (SLUG). *Nucleic Acids Res* 2013;**41**:6618–36. https://doi.org/10.1093/nar/gkt410
29. Elcheva IA, Wood T, Chiarolanzio K *et al.* RNA-binding protein IGF2BP1 maintains leukemia stem cell properties by regulating HOXB4, MYB, and ALDH1A1. *Leukemia* 2020;**34**:1354–63. https://doi.org/10.1038/s41375-019-0656-9
30. Dhamdhere MR, Gowda CP, Singh V *et al.* IGF2BP1 regulates the cargo of extracellular vesicles and promotes neuroblastoma metastasis. *Oncogene* 2023;**42**:1558–71. https://doi.org/10.1038/s41388-023-02671-0

31. Mahapatra L, Andruska N, Mao C *et al.* A novel IMP1 inhibitor, BTYNB, targets c-Myc and inhibits melanoma and ovarian cancer cell proliferation. *Transl Oncol* 2017;**10**:818–27. https://doi.org/10.1016/j.tranon.2017.07.008
32. Xiao P, Meng Q, Liu Q *et al.* IGF2BP1-mediated N6-methyladenosine modification promotes intrahepatic cholangiocarcinoma progression. *Cancer Lett* 2023;**557**:216075. https://doi.org/10.1016/j.canlet.2023.216075
33. Biegel JM, Dhamdhere M, Gao S *et al.* Inhibition of the mRNA-binding protein IGF2BP1 suppresses proliferation and sensitizes neuroblastoma cells to chemotherapeutic agents. *Front Oncol* 2021;**11**:608816. https://doi.org/10.3389/fonc.2021.608816
34. Liu Y, Guo Q, Yang H *et al.* Allosteric regulation of IGF2BP1 as a novel strategy for the activation of tumor immune microenvironment. *ACS Cent Sci* 2022;**8**:1102–15. https://doi.org/10.1021/acscentsci.2c00107
35. Wallis N, Oberman F, Shurrush K *et al.* Small molecule inhibitor of Igf2bp1 represses Kras and a pro-oncogenic phenotype in cancer cells. *RNA Biol* 2022;**19**:26–43. https://doi.org/10.1080/15476286.2021.2010983
36. Singh A, Singh V, Wallis N *et al.* Development of a specific and potent IGF2BP1 inhibitor: a promising therapeutic agent for IGF2BP1-expressing cancers. *Eur J Med Chem* 2024;**263**:115940. https://doi.org/10.1016/j.ejmech.2023.115940
37. Bley N, Schott A, Muller S *et al.* IGF2BP1 is a targetable SRC/MAPK-dependent driver of invasive growth in ovarian cancer. *RNA Biol* 2021;**18**:391–403. https://doi.org/10.1080/15476286.2020.1812894
38. Hsu PC, Yang CT, Jablons DM *et al.* The crosstalk between Src and Hippo/YAP signaling pathways in non-small cell lung cancer (NSCLC). *Cancers (Basel)* 2020;**12**:1361. https://doi.org/10.3390/cancers12061361
39. McNeish IA, Ledermann JA, Webber L *et al.* A randomised, placebo-controlled trial of weekly Paclitaxel and Saracatinib (AZD0530) in platinum-resistant ovarian, fallopian tube or primary peritoneal cancerdagger. *Ann Oncol* 2014;**25**:1988–95. https://doi.org/10.1093/annonc/mdu363
40. Puls LN, Eadens M, Messersmith W. Current status of SRC inhibitors in solid tumor malignancies. *Oncologist* 2011;**16**:566–78. https://doi.org/10.1634/theoncologist.2010-0408
41. Ramos R, Vale N. Dual drug repurposing: the example of Saracatinib. *Int J Mol Sci* 2024;**25**:4565. https://doi.org/10.3390/ijms25084565
42. McGivern N, El-Helali A, Mullan P *et al.* Activation of MAPK signalling results in resistance to Saracatinib (AZD0530) in ovarian cancer. *Oncotarget* 2018;**9**:4722–36. https://doi.org/10.18632/oncotarget.23524
43. Lamar JM, Xiao Y, Norton E *et al.* SRC tyrosine kinase activates the YAP/TAZ axis and thereby drives tumor growth and metastasis. *J Biol Chem* 2019;**294**:2302–17. https://doi.org/10.1074/jbc.RA118.004364
44. Ianevski A, Giri AK, Aittokallio T. SynergyFinder 3.0: an interactive analysis and consensus interpretation of multi-drug synergies across multiple samples. *Nucleic Acids Res* 2022;**50**:W739–43. https://doi.org/10.1093/nar/gkac382
45. Yadav B, Wennerberg K, Aittokallio T *et al.* Searching for drug synergy in complex dose-response landscapes using an interaction potency model. *Comput Struct Biotechnol J* 2015;**13**:504–13. https://doi.org/10.1016/j.csbj.2015.09.001
46. Sun WJ, Li JH, Liu S *et al.* RMBase: a resource for decoding the landscape of RNA modifications from high-throughput sequencing data. *Nucleic Acids Res* 2016;**44**:D259–65. https://doi.org/10.1093/nar/gkv1036
47. Xuan JJ, Sun WJ, Lin PH *et al.* RMBase v2.0: deciphering the map of RNA modifications from epitranscriptome sequencing data. *Nucleic Acids Res* 2018;**46**:D327–34. https://doi.org/10.1093/nar/gkx934
48. Livak KJ, Schmittgen TD. Analysis of relative gene expression data using real-time quantitative PCR and the 2(-Delta Delta C(T)) method. *Methods* 2001;**25**:402–8. https://doi.org/10.1006/meth.2001.1262
49. Robinson MD, McCarthy DJ, Smyth GK. edgeR: a Bioconductor package for differential expression analysis of digital gene expression data. *Bioinformatics* 2010;**26**:139–40. https://doi.org/10.1093/bioinformatics/btp616
50. Robinson MD, Oshlack A. A scaling normalization method for differential expression analysis of RNA-seq data. *Genome Biol* 2010;**11**:R25. https://doi.org/10.1186/gb-2010-11-3-r25
51. Subramanian A, Tamayo P, Mootha VK *et al.* Gene set enrichment analysis: a knowledge-based approach for interpreting genome-wide expression profiles. *Proc Natl Acad Sci USA* 2005;**102**:15545–50. https://doi.org/10.1073/pnas.0506580102
52. Liberzon A, Birger C, Thorvaldsdottir H *et al.* The Molecular Signatures Database (MSigDB) hallmark gene set collection. *Cell Syst* 2015;**1**:417–25. https://doi.org/10.1016/j.cels.2015.12.004
53. Galli GG, Carrara M, Yuan WC *et al.* YAP drives growth by controlling transcriptional pause release from dynamic enhancers. *Mol Cell* 2015;**60**:328–37. https://doi.org/10.1016/j.molcel.2015.09.001
54. Gyorffy B. Discovery and ranking of the most robust prognostic biomarkers in serous ovarian cancer. *GeroScience* 2023;**45**:1889–98. https://doi.org/10.1007/s11357-023-00742-4
55. Farina KL, Huttelmaier S, Musunuru K *et al.* Two ZBP1 KH domains facilitate beta-actin mRNA localization, granule formation, and cytoskeletal attachment. *J Cell Biol* 2003;**160**:77–87. https://doi.org/10.1083/jcb.200206003
56. Bankhead P, Loughrey MB, Fernandez JA *et al.* QuPath: open source software for digital pathology image analysis. *Sci Rep* 2017;**7**:16878. https://doi.org/10.1038/s41598-017-17204-5
57. Tothill RW, Tinker AV, George J *et al.* Novel molecular subtypes of serous and endometrioid ovarian cancer linked to clinical outcome. *Clin Cancer Res* 2008;**14**:5198–208. https://doi.org/10.1158/1078-0432.CCR-08-0196
58. Azar R, Susini C, Bousquet C *et al.* Control of contact-inhibition by 4E-BP1 upregulation. *Cell Cycle* 2010;**9**:1241–5. https://doi.org/10.4161/cc.9.7.11047
59. Wolf A, Krause-Gruszczynska M, Birkenmeier O *et al.* Plakophilin 1 stimulates translation by promoting eIF4A1 activity. *J Cell Biol* 2010;**188**:463–71. https://doi.org/10.1083/jcb.200908135
60. Degrauwe N, Suva ML, Janiszewska M *et al.* IMPs: an RNA-binding protein family that provides a link between stem cell maintenance in normal development and cancer. *Genes Dev* 2016;**30**:2459–74. https://doi.org/10.1101/gad.287540.116
61. Xia A, Yuan W, Wang Q *et al.* The cancer-testis lncRNA lnc-CTHCC promotes hepatocellular carcinogenesis by binding hnRNP K and activating YAP1 transcription. *Nat Cancer* 2022;**3**:203–18. https://doi.org/10.1038/s43018-021-00315-4
62. Sudol M, Bork P, Einbond A *et al.* Characterization of the mammalian YAP (Yes-associated protein) gene and its role in defining a novel protein module, the WW domain. *J Biol Chem* 1995;**270**:14733–41. https://doi.org/10.1074/jbc.270.24.14733
63. Wachter K, Kohn M, Stohr N *et al.* Subcellular localization and RNP formation of IGF2BPs (IGF2 mRNA-binding proteins) is modulated by distinct RNA-binding domains. *Biol Chem* 2013;**394**:1077–90. https://doi.org/10.1515/hsz-2013-0111
64. Weidensdorfer D, Stohr N, Baude A *et al.* Control of c-myc mRNA stability by IGF2BP1-associated cytoplasmic RNPs. *RNA* 2009;**15**:104–15. https://doi.org/10.1261/rna.1175909
65. Han S, Wang D, Tang G *et al.* Suppression of miR-16 promotes tumor growth and metastasis through reversely regulating YAP1 in human cholangiocarcinoma. *Oncotarget* 2017;**8**:56635–50. https://doi.org/10.18632/oncotarget.17832
66. Wu K, Chang F, Li W *et al.* Role of IGF2BPs in head and neck squamous cell carcinoma. *Front Oncol* 2022;**12**:1003808. https://doi.org/10.3389/fonc.2022.1003808

67. Karaman R, Halder G. Cell junctions in Hippo signaling. *Cold Spring Harb Perspect Biol* 2018;**10**:a028753. https://doi.org/10.1101/cshperspect.a028753
68. Si Y, Ji X, Cao X *et al.* Src inhibits the Hippo tumor suppressor pathway through tyrosine phosphorylation of Lats1. *Cancer Res* 2017;**77**:4868–80. https://doi.org/10.1158/0008-5472.CAN-17-0391
69. Luo J, Zou H, Guo Y *et al.* SRC kinase-mediated signaling pathways and targeted therapies in breast cancer. *Breast Cancer Res* 2022;**24**:99. https://doi.org/10.1186/s13058-022-01596-y
70. Szulzewsky F, Holland EC, Vasioukhin V. YAP1 and its fusion proteins in cancer initiation, progression and therapeutic resistance. *Dev Biol* 2021;**475**:205–21. https://doi.org/10.1016/j.ydbio.2020.12.018

Received: October 16, 2024. **Revised:** February 2, 2025. **Editorial Decision:** February 7, 2025. **Accepted:** February 13, 2025